Progress In Electromagnetics Research, Vol. 135, 391–410, 2013

WIP STUDY OF MULTIPLE METALLIC OBSTACLE SCATTERING

Nicolae Lucanu[1, *], Ion Bogdan[1], and Henri Baudrand[2]

[1]E.T.T.I. Faculty, Gh. Asachi Technical University of Iasi, Bd. Carol I No. 11, Iasi 700506, Romania

[2]ENSEEIHT, LAPLACE Laboratory, Institut National Polytechnique Toulouse, 2 Rue Camichel, Toulouse 31071, France

Abstract—The Wave Iterative Process is applied and validated for the study of the scattering of a plane wave by a multiple metallic dipole diffraction structure. The case of a single metallic dipole is treated, at first in normal incidence, than arbitrarily placed with respect to the incident wave. A double dipole scattering structure is studied, mutual influence being taken into account. The diffraction system is further enlarged to 5 randomly placed dipoles, the results issued from the WIP study being compared with those given by the Moments Method. Finally, the possibility of taking into account a very large number of dipoles is examined, by introducing an equivalent dipole distribution. The influence of this approximation on the WIP precision is presented.

1. INTRODUCTION

Recent years have witnessed a great development of the necessary tools able to numerically model, simulate the performance of, and design complex electromagnetic systems. Being used for nearly two decades, the Wave Iterative Process (WIP) is among the most efficient and easy to implement iterative methods, being applied to numerous types of electromagnetic problems.

Introduced in 1995 by Baudrand [1], the WIP was firstly developed as an instrument for the study of planar waveguide discontinuities scattering [2], active elements waveguide behavior being also modeled [3]. Due to its spatial-spectral combined formulation, the iterative method proved to be very computing efficient for the

Received 2 November 2012, Accepted 17 December 2012, Scheduled 26 December 2012

* Corresponding author: Nicolae Lucanu (nlucanu@etti.tuiasi.ro).

solving of electromagnetic problems involving multilayer microwave structures [4, 5].

The two dimension fast Fourier transform algorithm used at each iteration of WIP [6] proved to reduce the computing time and provide both the versatility and reliable representation of the circuit structure, making WIP an excellent study instrument for different types of planar antennas [7, 8]. Recent studies proved WIP to be very well adapted to the modeling of circular geometry antennas [9, 10].

Based upon a multiple reflection procedure, WIP is able to characterize structures of arbitrarily shaped patches deposited on multilayer isotropic/anisotropic dielectrics, making it particularly interesting for the study of frequency selective surfaces [11–14], EBG structures [15], and substrate integrated waveguides [16, 17], in the more general field of periodic and almost periodic structures [18–20].

The accuracy and efficiency of the WIP method depends on the relationship between the complexity of the circuits and the grid sizes chosen to model them. To increase computing effectiveness, a WIP multiscale approach formulation is used [21–24], resulting in the weak dependence of the calculation time with the circuit design.

One of the main advantages of the WIP is that it avoids the undesired phenomenon of unbounded operators; relations between currents and fields, obtained using unbounded impedance operators, are transposed to relations between waves, supplied by bounded scattering operators, having a less than unity modulus, the method's convergence being therefore always guaranteed. This determined the extension of the studied electromagnetic problems to free space scattering phenomena. Validated for some classic structures [25], the WIP was used to investigate free space diffraction by various single geometry obstacles [26–29].

Recent WIP studies focused on different ways of improving the speed of the iterative convergence, either by mesh adaptation through spectral connection [30], changes in the real domain operator [33], adoption of matrix-free solver [31], either by hybridization with other methods [32, 33].

In this work, an application of WIP to a multiple obstacle free space scattering problem is presented. The method is applied at first to a single dipole plane wave diffraction study, scattering operators and initial waves are determined, current density on the dipole length being calculated. The scattering structure in extended to a couple of arbitrarily placed metallic dipoles, in order to examine mutual radiation influence on the final dipole current density. The diffraction system is further enlarged to a 5 dipole structure, obtained results being compared with those issued by the Moments Method [34].

2. WAVE ITERATIVE PROCESS

Considered the incidence of a wave on the surface S of an obstacle as depicted in Fig. 1, the basic principle of the WIP is the concept of waves, the incident one A, and the reflected one B, defined from two dual quantities: current-voltage, electric field-magnetic field, volumetric density of current-electric field, charge's density-voltage, etc. For free space electromagnetic problems, transverse waves are defined from the tangent electric field E, and the incident magnetic tangent field H. For simplicity reasons, instead of H, the "current density" vector J is preferred. The following relation defines the J vector:

$$\vec{J} = \vec{H} \times \hat{n} \tag{1}$$

where $\hat{n}$ is the normal versor to the scattering surface, defined in each point.

The waves A and B are defined by (2):

$$\begin{cases} \vec{A} = \frac{1}{2\sqrt{Z_0}} \left(\vec{E} + Z_0 \vec{J} \right) \\ \vec{B} = \frac{1}{2\sqrt{Z_0}} \left(\vec{E} - Z_0 \vec{J} \right) \end{cases} \tag{2}$$

where Z_0 is an arbitrary parameter.

The analytic expression of the iterative process is issued from the continuity and border conditions on the electromagnetic field. In the case of free space scattering, the iterative process is described by (3):

$$\begin{cases} \vec{B}_n + \vec{B}_0 = \hat{S} \left(\vec{A}_{n-1} + \vec{A}_0 \right) \\ \vec{A}_n = \hat{\Gamma} \vec{B}_n \end{cases} \tag{3}$$

where n is the number of the iteration, $\hat{S}$ the real domain scattering operator, and $\hat{\Gamma}$ the modal domain scattering operator.

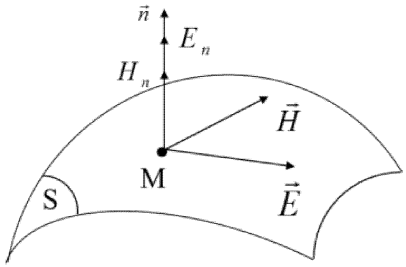

Figure 1. Scattering surface with vector definitions.

The real domain scattering operator is given by (4):

$$\hat{S} = I_S - I_M \tag{4}$$

where I_S and I_M are the dielectric and respectively metallic domain definition functions, defined as:

$$I_M = \begin{cases} 1 & \text{on the metallic domain} \\ 0 & \text{elsewhere} \end{cases} \tag{5}$$

and, respectively:

$$I_S = \begin{cases} 1 & \text{on the dielectric domain} \\ 0 & \text{elsewhere}l \end{cases} \tag{6}$$

The modal domain scattering operator is determined from:

$$\vec{J} = \hat{Y}\vec{E} \tag{7}$$

where $\hat{Y}$ is the admittance operator defined as:

$$\hat{Y} = \sum_m |f_m\rangle\, Y_m\, \langle f_m| \tag{8}$$

where $\{f_m\}$ is a complete orthonormal modal base and Y_m the modal admittance of the mth mode. The bra-ket writing convention is used, and $|f_m\rangle$ denotes the function itself, while $\langle f_m|$ has the meaning of "scalar product with".

The modal domain scattering operator is expressed as the sum of the reflection coefficient of the modes and is given by:

$$\hat{\Gamma} = \sum_m |f_m\rangle\, \frac{1 - Z_0 Y_m}{1 + Z_0 Y_m}\, \langle f_m| \tag{9}$$

The first equation of (3) is written in the real domain, the second one written in the spectral domain, and therefore direct and inverse fast modal (*Fourier*) transformations (FFT and FFT^{-1}) are used to pass from one to the other.

A_0 and B_0 are the waves corresponding to the incident electromagnetic field on the studied structure, defined as:

$$\begin{cases} \vec{A}_0 = \frac{1}{2\sqrt{Z_0}} \left(\vec{E}^i + Z_0 \vec{J}^i\right) \\ \vec{B}_0 = \frac{1}{2\sqrt{Z_0}} \left(\vec{E}^i - Z_0 \vec{J}^i\right) \end{cases} \tag{10}$$

Once the iterative process is accomplished, the electric field and the current density can be calculated using the inverse relations of (2), that is:

$$\begin{cases} \vec{E} = \sqrt{Z_0} \left(\vec{A} + \vec{B}\right) \\ \vec{J} = \frac{1}{\sqrt{Z_0}} \left(\vec{A} - \vec{B}\right) \end{cases} \tag{11}$$

A schematic of the current density calculation on the scatterer's surface using the WIP is presented in Fig. 2.

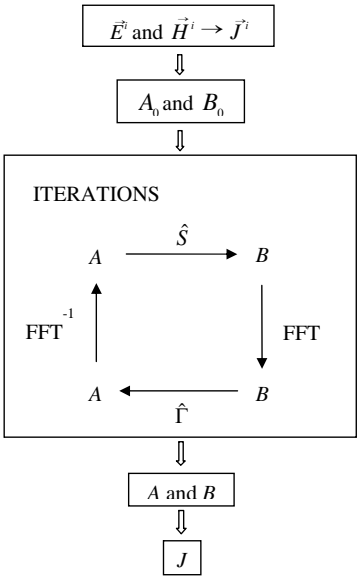

Figure 2. Schematic of the iterative process.

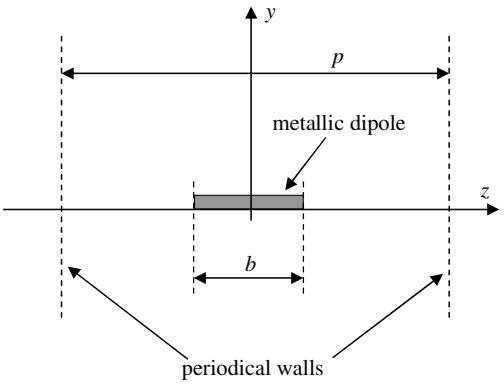

Figure 3. Metallic dipole between periodical walls.

3. SCATTERING BY A METALLIC DIPOLE — NORMAL INCIDENCE

Let us consider a metallic dipole, placed along the z axis, illuminated by a 10 GHz plane wave with a normal incidence, as shown in Fig. 3. The geometrical dimensions of the dipole are a radius a of 12.5 µm and a length b of 15 mm. Its axis is z-oriented.

The study of the dipole scattering would theoretically involve an infinity of points following the z axis, which is numerically impossible. That is why we introduced a first approximation, considering the structure as periodical, the dipole being placed in the middle of the p period.

The metallic (electric wall) domain function is given by:

$$I_M(z) = \begin{cases} 1 & \text{if } z \in \left[-\frac{b}{2}, \frac{b}{2}\right] \\ 0 & \text{elsewhere} \end{cases} \tag{12}$$

I_S is the complementary function, defining the magnetic wall domain:

$$I_S(z) = \begin{cases} 0 & \text{if } z \in \left[-\frac{b}{2}, \frac{b}{2}\right] \\ 1 & \text{elsewhere} \end{cases} \tag{13}$$

Due to the periodicity of the structure, the expressions of the

functions of the modal base are given by:

$$\langle f_m(z)| = a_m e^{-j\frac{2\pi}{p}mz} \tag{14}$$

where a_m is determined by the othonormation condition:

$$\langle f_m \mid f_m \rangle = 1 \tag{15}$$

Its value results:

$$a_m = \frac{1}{\sqrt{p}} \tag{16}$$

The modal admittance derives from the expression of the cylindrical modes [35]:

$$Y_m = \frac{\gamma_m}{j\omega\mu} \frac{H_n^{(2)}(\gamma_m a)}{H_n^{(2)'}(\gamma_m a)} \tag{17}$$

where $H_n^{(2)}$ is the second kind *Hankel* function.

Taking into account the very small size of the radius, we can write:

$$Y_m = \frac{\gamma_m}{j\omega\mu} \frac{B_0(\gamma_m a)}{B_0'(\gamma_m a)} \tag{18}$$

where

$$\gamma_m = \sqrt{\left(\frac{2\pi m}{p}\right)^2 - k_0^2} \tag{19}$$

k_0 is the wavenumber and B_0 traduces:

$$B_0(\gamma_m a) = \begin{cases} H_0^{(2)}(\gamma_m a) & \text{if} \quad \gamma_m \in IR \\ \frac{2j}{\pi} K_0(j\gamma_m a) & \text{if} \quad \gamma_m \in iIR \end{cases} \tag{20}$$

where K_0 is the second kind modified Bessel function.

Considering the incident plane wave as x-polarized, the incident electromagnetic field is given by:

$$\begin{cases} E^i = E_0 e^{-jk_0 z} \\ J^i = H_0 I_M e^{-jk_0 z} \end{cases} \tag{21}$$

where I_M is the dipole definition function (12), and E_0 and H_0 are the amplitudes.

The waves used for the initialization of the iterative process are given by:

$$\begin{cases} A_0 = \frac{1}{2\sqrt{Z_0}} (E_0 + Z_0 H_0 I_M) e^{-jk_0 z} \\ B_0 = \frac{1}{2\sqrt{Z_0}} (E_0 - Z_0 H_0 I_M) e^{-jk_0 z} \end{cases} \tag{22}$$

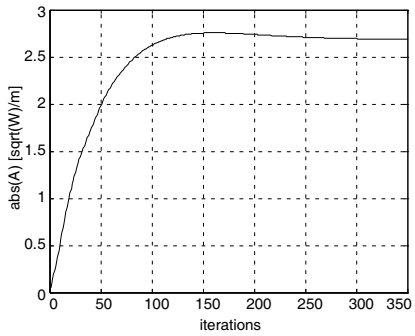

Figure 4. Iterative convergence of the A wave.

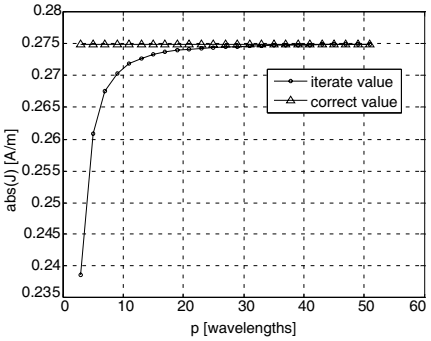

Figure 5. Period size influence on the result precision.

Taking into account the small size of the radius of the dipole, we expect [25] a quite large number of iterations to be done in order to obtain a correct result. On the other hand, due to the small geometric dimensions of the structure, only 2 modes are needed to correctly describe the modal behavior, determining an overall very good computational cost, mainly because of the FFT speed gain.

Figure 4 presents the evolution of A wave with the number of iterations. As we expected, due to very small size of the radius, a big number of iterations is necessary in order to achieve the convergence iteration stop criteria. At least 250 iterations must be made for an accurate result, meaning less than 1% variation of the absolute value of the A and B waves between two consecutive iterations.

Figure 5 presents the study of the size of the period p that must be considered between two walls. The current density is evaluated in the center of the dipole, at the point $z = 0$. A period of 30 wavelengths is sufficient for a better than 1% precision.

Figure 6 presents the aspect of the current density on the dipole length, evaluated using WIP and using the Moments Method. The results are in very good accord.

4. SCATTERING BY A METALLIC DIPOLE — ARBITRARY INCIDENCE

In the following, we shall continue the study by placing the dipole in an arbitrary inclination with respect to the incident wave [36]. The situation is depicted in Fig. 7.

The rectangular coordinates system was chosen as oriented after the incident wave. The geometrical position of the dipole is described

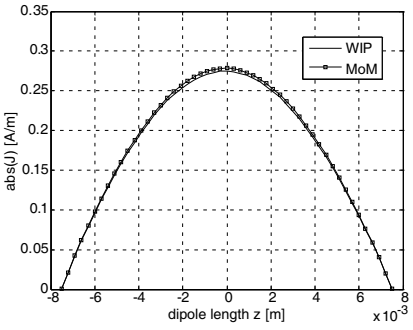

Figure 6. Current density on the dipole length.

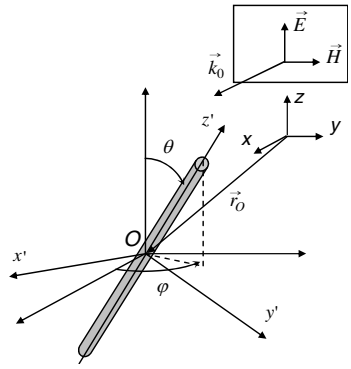

Figure 7. Metallic dipole — arbitrary incidence.

using the coordinates of the center O and the two inclination angles θ with respect to the z axis and φ with respect to the x axis. The dipole's geometric position is therefore entirely described by:

$$d: \quad \left(\vec{r}_O \left\{ \begin{array}{c} x_O \\ y_O \\ z_O \end{array} \right. \quad \theta \quad \varphi \right) \tag{23}$$

This way of describing the geometrical position of the dipole presents the advantage of the possibility of taking into account a multiple dipole scattering structure.

Let us denote the coordinates system proper to the dipole (Fig. 7) as (x', y', z'). The incident electromagnetic field is given in the new coordinates system by:

$$\vec{E}^i = E_0 e^{-jk_0 x_O} e^{-jk'_x x'} e^{-jk'_y y'} e^{-jk'_z z'} \cos\theta \cdot \vec{z}' \tag{24}$$

where the following notations are made:

$$k'_x = k_0 \cos\varphi \cos\theta \tag{25}$$

$$k'_y = k_0 \sin\varphi \cos\theta \tag{26}$$

$$k'_z = k_0 \sin\theta \tag{27}$$

Due to the small size of the radius, we can approximate (24):

$$\vec{E}^i = E_0 e^{-jk_0 x_O} e^{-jk'_z z'} \cos\theta \cdot \vec{z}' \tag{28}$$

Denoting the new amplitude:

$$E'_0 = E_0 e^{-jk_0 x_O} \cos\theta \tag{29}$$

the values of the incident electromagnetic field become similar to (17):

$$\begin{cases} E^i = E'_0 e^{-jk'_z z'} \\ J^i = H'_0 I_M e^{-jk'_z z'} \end{cases} \tag{30}$$

and the expressions of the initialization waves are given by:

$$\begin{cases} A_0 = \frac{1}{2\sqrt{Z_0}} \left(E'_0 + Z_0 H'_0 I_M\right) e^{-jk'_z z'} \\ B_0 = \frac{1}{2\sqrt{Z_0}} \left(E'_0 - Z_0 H'_0 I_M\right) e^{-jk'_z z'} \end{cases} \tag{31}$$

Figure 8 presents the results for the case of an inclined dipole, described by:

$$d: \quad \left(\vec{r}_O \begin{cases} \lambda \\ \lambda \\ \lambda \end{cases} \quad 30^\circ \quad 45^\circ \right) \tag{32}$$

where λ is the wavelength.

The current density is calculated using both WIP and Method of Moments, the two approaches giving very close results.

5. SCATTERING BY TWO ARBITRARILY PLACED METALLIC DIPOLES

Let us consider a diffraction structure formed by two metallic dipoles, being arbitrarily placed and having arbitrary inclinations with respect to the incident plane wave, as described in Fig. 9.

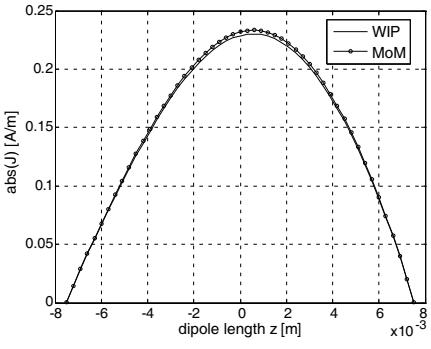

Figure 8. Current density on an inclined dipole.

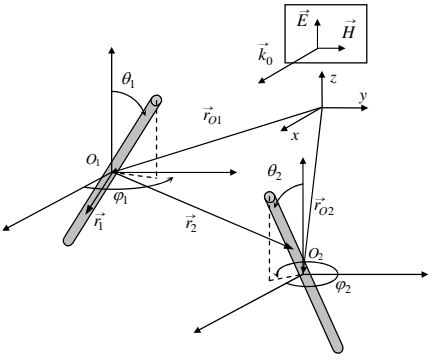

Figure 9. Two arbitrarily placed metallic dipoles.

The geometrical position of the dipoles is described in the same manner as (23), that is:

$$d_1\text{:}\left(\vec{r}_{O1}\left\{\begin{array}{l} x_{O1} \\ y_{O1} \\ z_{O1}\end{array}\right.\quad \theta_1 \quad \varphi_1\right) \text{ and } d_2\text{:}\left(\vec{r}_{O2}\left\{\begin{array}{l} x_{O2} \\ y_{O2} \\ z_{O2}\end{array}\right.\quad \theta_2 \quad \varphi_2\right) \tag{33}$$

The current densities induced by the incident plane wave on each dipole are calculated in the same manner as presented in the previous paragraph, the 2 dipoles being independently studied.

We are now interested in evaluating the influence of the current density on the first dipole on the second one. For this, we need to know the electric field radiated by the first dipole on the second one.

In order to evaluate the radiated electric field by the current density due to the incident wave on the first dipole, at the level of the second dipole, we shall use the vector potential $\vec{A}(\vec{r}_2)$:

$$\vec{A}(\vec{r}_2) = \frac{1}{4\pi}\int\limits_{l_1} \vec{J}_1(\vec{r}_1)\,\frac{e^{-jk_0|\vec{r}_2-\vec{r}_1|}}{|\vec{r}_2-\vec{r}_1|}dl_1 \tag{34}$$

where $\vec{J}_1(\vec{r}_1)$ represents the density current inducted by the incident plane wave on the length l_1 of the first dipole.

The electric field radiated by the first dipole on the second one is given by:

$$\vec{E}_{12}(\vec{r}_2) = -j\omega\mu_0 \cdot \vec{A}(\vec{r}_2) + \frac{1}{j\omega\varepsilon_0}\cdot\nabla_2\left[\nabla_2\cdot\vec{A}(\vec{r}_2)\right] \tag{35}$$

where the subscript 2 of the ∇ operator designates the fact that all derivation operations are made with respect to the second dipole own coordinates system.

We inject (35) in (34) and we obtain:

$$\begin{aligned}\vec{E}_{12}(\vec{r}_2) \;=\; & -j\omega\mu_0\cdot\frac{1}{4\pi}\int\limits_{l_1}\vec{J}_1(\vec{r}_1)\frac{e^{-jk_0|\vec{r}_2-\vec{r}_1|}}{|\vec{r}_2-\vec{r}_1|}dl_1 \\ & +\frac{1}{j\omega\varepsilon_0}\cdot\frac{1}{4\pi}\int\limits_{l_1}\vec{J}_1(\vec{r}_1)\nabla_2\left[\nabla_2\cdot\left(\frac{e^{-jk_0|\vec{r}_2-\vec{r}_1|}}{|\vec{r}_2-\vec{r}_1|}\right)\right]dl_1\end{aligned} \tag{36}$$

Once the derivation operations are done, the integrals in (36) must be numerically evaluated, since $\vec{J}_1$ is numerically calculated. The terms

of Equation (35) become:

$$\vec{A}(\vec{r}_2) = \frac{1}{4\pi}\left(\int_{l_1} J_1 \sin\theta_1 \cos\varphi_1 \frac{e^{-jk_0 d}}{d} dl_1 \cdot \vec{x}_2 + \int_{l_1} J_1 \sin\theta_1 \sin\varphi_1 \frac{e^{-jk_0 d}}{d} dl_1 \cdot \vec{y}_2 + \int_{l_1} J_1 \cos\theta_1 \frac{e^{-jk_0 d}}{d} dl_1 \cdot \vec{z}_2\right) \quad (37)$$

and, respectively:

$$\nabla_2\left[\nabla_2 \cdot \vec{A}(\vec{r}_2)\right] = \frac{1}{4\pi}\left(dA_x \cdot \vec{x}_2 + dA_y \cdot \vec{y}_2 + dA_z \cdot \vec{z}_2\right) \quad (38)$$

with the following notations:

$$dA_x = \int_{l_1} J_1 \frac{e^{-jk_0 d}}{d}\left[\left(-jk_0 - \frac{1}{d}\right)\sin\theta_1 \cos\varphi_1 + w(x_2 - x_1)\frac{1}{d^4}\left(-k_0^2 d - jk_0 - \frac{1}{d}\right)\right] dl_1 \quad (39)$$

$$dA_y = \int_{l_1} J_1 \frac{e^{-jk_0 d}}{d}\left[\left(-jk_0 - \frac{1}{d}\right)\sin\theta_1 \sin\varphi_1 + w(y_2 - y_1)\frac{1}{d^4}\left(-k_0^2 d - jk_0 - \frac{1}{d}\right)\right] dl_1 \quad (40)$$

$$dA_z = \int_{l_1} J_1 \frac{e^{-jk_0 d}}{d}\left[\left(-jk_0 - \frac{1}{d}\right)\cos\theta_1 + w(z_2 - z_1)\frac{1}{d^4}\left(-k_0^2 d - jk_0 - \frac{1}{d}\right)\right] dl_1 \quad (41)$$

where the following notations are used:

$$d = \sqrt{(x_2 - x_1)^2 + (y_2 - y_1)^2 + (z_2 - z_1)^2} \quad (42)$$

$$w = (x_2 - x_1)\sin\theta_1 \cos\varphi_1 + (y_2 - y_1)\sin\theta_1 \sin\varphi_1 + (z_2 - z_1)\cos\theta_1 \quad (43)$$

The generated magnetic field by the current distribution on the second dipole is given by:

$$\vec{H}_{12}(\vec{r}_2) = \nabla_2 \times \vec{A}(\vec{r}_2) \quad (44)$$

Once we have the radiated electromagnetic field by the first dipole on the second one, we realize the iterative process by the steps presented in Fig. 2.

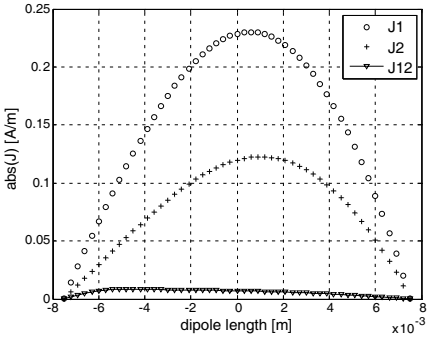

Figure 10. Current densities on two inclined dipoles and mutual influence of the first on the second one.

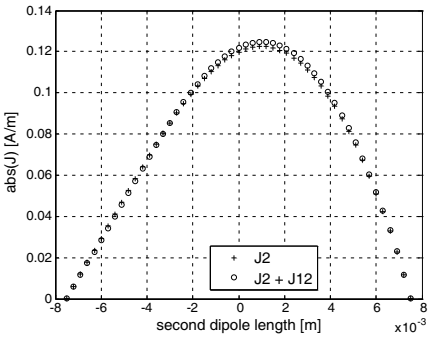

Figure 11. Current density on the second dipole with and without the mutual influence of the first one.

Let us now consider two metallic dipoles, geometrically given by:

$$d_1\text{:}\quad \left(\vec{r}_{O1} \begin{cases} x_{O1} = \lambda \\ y_{O1} = \lambda \\ z_{O1} = \lambda \end{cases} \quad \theta_1 = 30^\circ \quad \varphi_1 = 45^\circ \right) \tag{45}$$

$$d_2\text{:}\quad \left(\vec{r}_{O2} \begin{cases} x_{O2} = \left(1 + 1/\sqrt{3}\right)\lambda \\ y_{O2} = \left(1 + 1/\sqrt{3}\right)\lambda \\ z_{O2} = \left(1 + 1/\sqrt{3}\right)\lambda \end{cases} \quad \theta_2 = 60^\circ \quad \varphi_2 = 30^\circ \right) \tag{46}$$

The positions of the two dipoles were chosen so that between the two centres we have a one wavelength λ distance.

Figure 10 presents the current densities on the two dipoles due to the incident plane wave, as well as the influence of the first dipole on the second one. Each of the three presented results needs the same computational cost as the single dipole from Section 1.

In order to visualize the order of the influence of the first dipole on the second one, we represent in Fig. 11 the current density on the second dipole, with and without the radiation due to the first one.

One can notice that although the mutual influence has a low level, it cannot be neglected, especially if a multiple dipole scattering structure is to be taken into study.

6. SCATTERING BY 5 METALLIC DIPOLES

The incidence of a 10 GHz plane wave on the surface of a 5 dipole scattering system is considered, each dipole having the radius $a =$

12.5 [μm] and the length is $b = 0.015$ [m]. The 5 dipoles have the positions given by a positioning program, after being thrown from a common departure point:

$$d_1: \quad \left(\vec{r}_{O1} \begin{cases} x_{O1} = 0.128882 \\ y_{O1} = 0.056478 \\ z_{O1} = 0.028073 \end{cases} \quad \varphi_1 = 181.909^\circ \quad \theta_1 = 90.893^\circ \right) \tag{47}$$

$$d_2: \quad \left(\vec{r}_{O2} \begin{cases} x_{O2} = 0.137477 \\ y_{O2} = 0.179280 \\ z_{O2} = 0.036709 \end{cases} \quad \varphi_2 = 237.896^\circ \quad \theta_2 = 140.042^\circ \right) \tag{48}$$

$$d_3: \quad \left(\vec{r}_{O3} \begin{cases} x_{O3} = 0.021855 \\ y_{O3} = 0.148254 \\ z_{O3} = 0.138456 \end{cases} \quad \varphi_3 = 55.226^\circ \quad \theta_3 = 84.789^\circ \right) \tag{49}$$

$$d_4: \quad \left(\vec{r}_{O4} \begin{cases} x_{O4} = 0.089868 \\ y_{O4} = 0.025445 \\ z_{O4} = 0.042779 \end{cases} \quad \varphi_4 = 224.665^\circ \quad \theta_4 = 229.537^\circ \right) \tag{50}$$

$$d_5: \quad \left(\vec{r}_{O5} \begin{cases} x_{O5} = 0.004324 \\ y_{O5} = 0.053995 \\ z_{O5} = 0.186783 \end{cases} \quad \varphi_5 = 291.224^\circ \quad \theta_5 = 245.944^\circ \right) \tag{51}$$

Fig. 12 presents the current densities on the 5 dipoles lengths, calculated using WIP and using the Moments Method. 5 complete iterative procedures need to be done for each dipole (the initial independent current density calculation and 4 mutual influence evaluations).

The results given by WIP are in very good accordance with the ones issued from the Method of Moments, the computational time when using Matlab about 25% lower.

7. EQUIVALENT DIPOLE APPROXIMATION

In the following, the introduction of a useful approximation is examined. Let us consider the dipole from Fig. 7, having the current density distribution issued from the application of the WIP.

The dipole is replaced by three "equivalent" dipoles, having the same length b as the original, oriented after each of the three axis of the coordinates system, as described in Fig. 13.

The current densities on the equivalent dipoles are equal to the

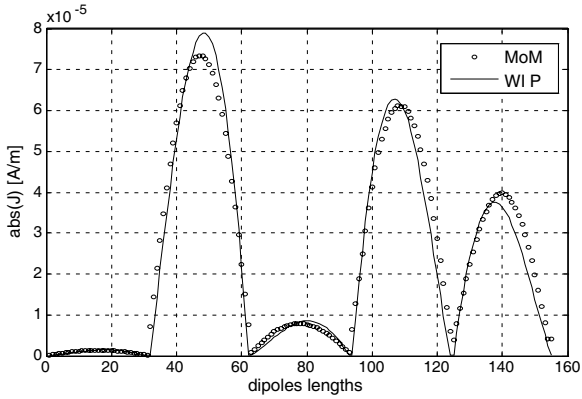

Figure 12. Current densities on the 5 diploes.

components of $\vec{J}$ present on the main dipole:

$$\vec{J} = \vec{J}_x + \vec{J}_y + \vec{J}_z \tag{52}$$

where J_x, J_y, and J_z are the projections of J on the three axes.

$$\vec{J}_x = J \sin\theta \cos\varphi \cdot \vec{x} \tag{53}$$

$$\vec{J}_y = J \sin\theta \sin\varphi \cdot \vec{y} \tag{54}$$

$$\vec{J}_z = J \cos\theta \tag{55}$$

Since both electric and magnetic fields generated by the current distribution on a dipole can be evaluated using the vector potential $\vec{A}$, this will be the target of the study in order to evaluate the precision of the dipole equivalence.

The vector potential induced to the point $\vec{r}_2$ by a dipole is defined by [35]:

$$\vec{A}\,(\vec{r}_2) = \frac{1}{4\pi} \int_{-b/2}^{b/2} \vec{J}(\vec{r}_1) \frac{e^{-jk_0|\vec{r}_2 - \vec{r}_1|}}{|\vec{r}_2 - \vec{r}_1|} dl \tag{56}$$

Each of the three equivalent dipoles creates a vector potential given by:

$$\vec{A}_i\,(\vec{r}_2) = \frac{1}{4\pi} \int_{-b/2}^{b/2} \vec{J}_i(\vec{r}_1) \frac{e^{-jk_0|\vec{r}_2 - \vec{r}_1|}}{|\vec{r}_2 - \vec{r}_1|} di \tag{57}$$

where i is x, y, and, respectively z.

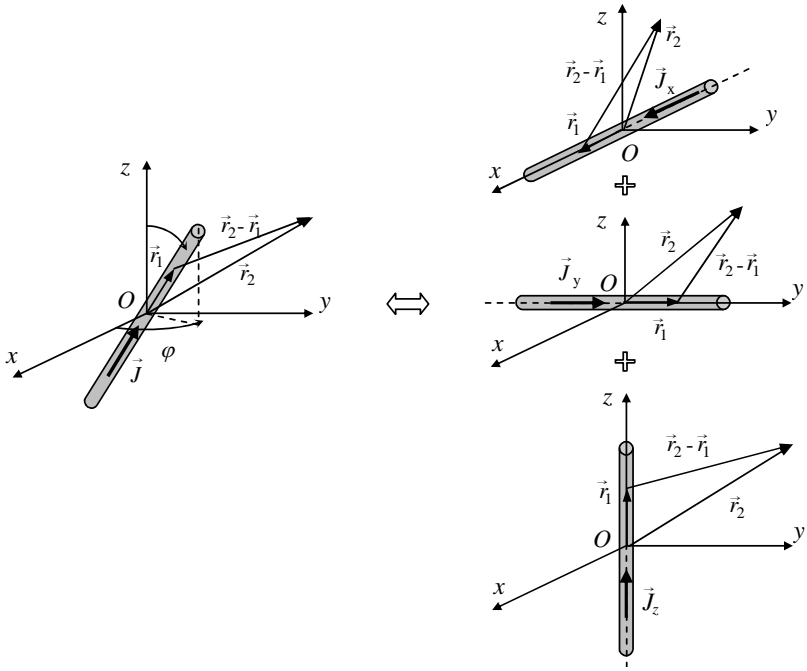

Figure 13. Equivalent dipole distribution.

The following approximation needs to be evaluated, in order to draw a conclusion on the dipole distribution radiation equivalence:

$$\vec{A}\left(\vec{r}_2\right) = \sum_i \vec{A}_i\left(\vec{r}_2\right) \tag{58}$$

The approximation (58) mathematically holds for far-field radiation, near-field case being numerically investigated bellow.

The introduction of the equivalent dipole distribution will allow the study of multiple dipole scattering structures [37], as suggested for a 2D obstacle distribution in Fig. 14.

Figure 15 presents the evolution with the distance of the percentage error e_p on the vector potential $\vec{A}$ due to the equivalent dipole approximation.

The percentage error is evaluated using the following relation:

$$e_p = \frac{\left|\vec{A}_{aprox}\right| - \left|\vec{A}_{cor}\right|}{\left|\vec{A}_{cor}\right|} \cdot 100 \tag{59}$$

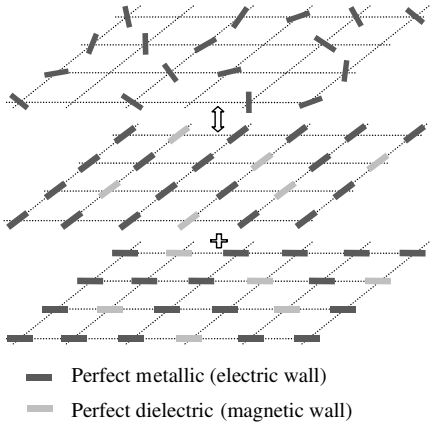

Figure 14. Multiple 2D structure — equivalent axis-oriented dipoles.

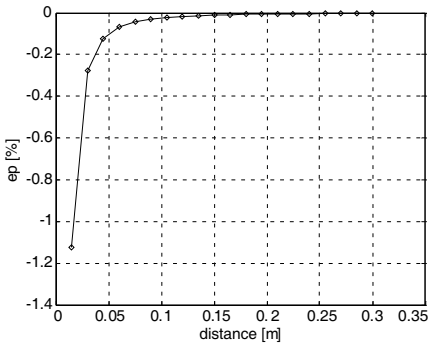

Figure 15. Approximation percentage error.

where $\vec{A}_{cor}$ is the correct value (56), and $\vec{A}_{approx}$ is the sum of the three equivalent dipoles vector potentials (58). The distance is measured from the center of the dipole. The same dipole from Section 4 defined by (32) is considered, the evaluating radiation direction being along the y axis.

One can notice the very low rate of the error, both for the near field calculations and for the far field estimation.

8. CONCLUSION

An application of the WIP was realized for different metallic dipoles structures, starting with the classic case of the normal incidence, and finishing with a 5-dipole arbitrary structure. WIP results proved to be in very good concordance with those issued from the Moments Method, allowing us to validate the iterative method for 3D multiple scatterers. The possibility of further enlarging the number of dipoles in the scattering structure was examined, a useful approximation being introduced, in order to allow WIP application to the problem of very large multiple diffraction structures.

ACKNOWLEDGMENT

The authors would like to thank Professor G. Chassay from IETR of INSA Rennes France for the Moments Method results.

This paper was supported by the project PERFORM-ERA "Postdoctoral Performance for Integration in the European Research Area" (ID-57649), financed by the European Social Fund and the Romanian Government.

REFERENCES

1. Azizi, M., H. Aubert, and H. Baudrand, "A new iterative method for scattering problems," *Proc. of 25th European Microwave Conference*, 255–258, Bologna, Italy, Sep. 1995.
2. Azizi, M., M. Boussouis, H. Aubert, and H. Baudrand, "A three-dimensional analysis of planar discontinuities by an iterative method," *Microwave and Optical Technology Letters*, Vol. 13, No. 6, 372–376, Dec. 1996.
3. Sboui, N., A. Gharsallah, A. Gharbi, and H. Baudrand, "Global modelling of microwave active circuits by an efficient iterative procedure," *IEE Proceedings Microwave and Antennas Propagation*, Vol. 148, No. 3, 209–212, Jun. 2001.
4. Wane, S., D. Bajon, H. Baudrand, and P. Gamand, "A new full-wave hybrid differential-integral approach for the investigation of multilayer structures including nonuniformly doped diffusions," *IEEE Trans. Microwave Theory and Techniques*, Vol. 53, No. 1, 200–214, Jan. 2005.
5. Hajlaoui, E. A., H. Trabelsi, H. Zairi, A. Gharsallah, and H. Baudrand, "Analysis of multilayer substrates by multilayer contribution of wave concept iterative process," *Microwave and Optical Technology Letters*, Vol. 49, No. 6, 1439–1445, Jun. 2007.
6. N'Gongo, R. S. and H. Baudrand, "A new approach for microstrip active antennas using modal F.F.T-algorithm," *IEEE Antennas and Propagation Int. Symp.*, Vol. 3, 1700–1703, Orlando, USA, Jul. 1999.
7. Richalot, E., M. F. Wong, H. Baudrand, and V. Fouad-Hanna, "Modeling of arbitrary shaped radiating structures by the wave concept iterative process," *2000 IEEE MTT-S International Microwave Symposium Digest*, Vol. 1, 113–116, Jun. 2000.
8. D'Assuncao, Jr., A. G., G. Fontgalland, M. Titaouine, H. Baudrand, D. N. Meireles, and A. G. Neto, "Analysis of tapered micostrip patch antenna by the wave concept iterative procedure," *Proc. of 2009 SBMO/IEEE MTT-S International Microwave & Optoelectronics Conference (IMOC 2009)*, 62–66, Belem, Brasil, Nov. 2009.
9. Wang, Y., Y. J. Xie, and H. Feng, "Analysis of cylindrically

conformal microstrip structures using an iterative method," *Progress In Electromagnetics Research*, Vol. 87, 215–231, 2008.

10. Houaneb, Z., H. Zairi, A. Gharsallah, and H. Baudrand, "Modeling of cylindrical resonators by wave concept iterative process in cylindrical coordinates," *International Journal of Numerical Modelling: Electronic Networks, Devices and Fields*, Vol. 24, No. 2, 123–131, Mar.–Apr. 2011.
11. Titaouine, M., A. G. Neto, H. Baudrand, and F. Djahli, "Analysis of frequency selective surface on isotropic/anisotropic layers using WCIP method," *ETRI Journal*, Vol. 29, No. 1, 36–44, Feb. 2007.
12. Titaouine, M., A. G. Neto, H. Baudrand, and F. Djahli, "Determination of metallic ring FSS scattering characteristics using WCIP method," *Microwave and Optical Technology Letters*, Vol. 50, No. 5, 1324–1328, May 2008.
13. Costa, F., S. Genovesi, and A. Monorchio, "A frequency selective absorbing ground plane for low-RCS microstrip antenna arrays," *Progress In Electromagnetics Research*, Vol. 126, 317–332, 2012.
14. Su, J., X.-W. Xu, M. He, and K. Zhang, "Integral-equation analysis of frequency selective surfaces using Ewald transformation and lattice symmetry," *Progress In Electromagnetics Research*, Vol. 121, 249–269, 2011.
15. Jandieri, V., K. Yasumoto, and Y.-K. Cho, "Rigorous analysis of electromagnetic scattering by cylindrical EBG structures," *Progress In Electromagnetics Research*, Vol. 121, 317–342, 2011.
16. Alhzzoury, A. I., N. Raveu, O. Pigaglio, H. Baudrand, and K. Al-Abdullah, "WCIP applied to substrate integrated waveguide," *Progress In Electromagnetics Research C*, Vol. 33, 171–184, 2012.
17. Zhang, Q.-L., W.-Y. Yin, S. He, and L.-S. Wu, "Evanescent-mode substrate integrated waveguide (SIW) filters implemented with complementary split ring resonators," *Progress In Electromagnetics Research*, Vol. 111, 419–432, 2011.
18. Baudrand, H., M. Titaouine, N. Raveu, and G. Fontgland, "Electromagnetic modeling of planar almost periodic structures," *Proc. of 2009 SBMO/IEEE MTT-S International Microw. & Optoelectronics Conference (IMOC 2009)*, 427–431, Belem, Brasil, Nov. 2009.
19. Kusiek, A., R. Lech, and J. Mazur, "Analysis of electromagnetic plane wave scattering from 2-D periodic arrangements of posts," *Progress In Electromagnetics Research*, Vol. 129, 69–90, 2012.
20. Xiao, K., F. Zhao, S.-L. Chai, J.-J. Mao, and J. L.-W. Li, "Scattering analysis of periodic arrays using combined CBF/P-

FFT method," *Progress In Electromagnetics Research*, Vol. 115, 131–146, 2011.

21. Cohen, L., R. S. N'Gongo, R. Garcia, and H. Baudrand, "Equivalent impedance boundary conditions for refined meshes applied to planar circuits," *IEE Proc. — Microw. Antennas Propag.*, Vol. 150, No. 4, 237–243, Aug. 2003.
22. Zairi, H., A. Gharsallah, A. Gharbi, and H. Baudrand, "Analysis of planar circuits using a multigrid iterative method," *IEE Proc. — Microw. Antennas Propag.*, Vol. 153, No. 3, 231–236, Jun. 2006.
23. Baudrand, H., N. Raveu, N. Sboui, and G. Fontgalland, "Applications of multiscale waves concept iterative procedure," *Proc. of 2007 SBMO/IEEE MTT-S International Microw. & Optoelectronics Conference (IMOC 2007)*, 749–752, Salvador, Brasil, Nov. 2007.
24. Raveu, N., G. Prigent, O. Pigaglio, and H. Baudrand, "Different spectral scale level in the wave concept iterative procedure to solve multi-scale problems," *IET Microw. Antennas Propag.*, Vol. 4, No. 9, 1247–1255, Sep. 2010.
25. Lucanu, N., I. V. Pletea, I. Bogdan, and H. Baudrand, "Wave concept iterative method validation for 2D metallic obstacles scattering," *Advances in Electrical and Computer Engineering*, Vol. 12, No. 1, 9–14, Feb. 2012
26. Zeid, A. and H. Baudrand, "Electromagnetic scattering by metallic holes and its applications in microwave circuit design," *IEEE Trans. Microwave Theory and Techniques*, Vol. 50, No. 4, 1198–1206, Apr. 2002.
27. Raveu, N., T. P. Vuong, I. Terrasse, G.-P. Piau, and H. Baudrand, "Near fields evaluated with the wave concept iterative procedure method for an E-polarisation plane wave scattered by cylindrical strips," *Microw. and Optical Tech. Letters*, Vol. 38, No. 5, 403–406, Sep. 2003.
28. Ammar, N., T. Aguili, and H. Baudrand, "Analysis of multilayered cylindrical structures using a full wave method," *Progress In Electromagnetics Research*, Vol. 85, 425–438, 2008.
29. Raveu, N., O. Pigaglio, G. Prigent, and H. Baudrand, "Improvement in the wave concept iterative procedure through spectral connection," *Proceedings of the 37th European Microwave Conference*, 28–31, Munich, Germany, Oct. 2007.
30. Raveu, N. and H. Baudrand, "Improvement of the WCIP convergence," *Proc. IEEE Antennas and Propagation Society International Symposium APSURSI'09*, 1–4, Charleston, USA, Jun. 2009.

31. Raveu, N., L. Giraud, and H. Baudrand, "WCIP acceleration," *Proc. Asia-Pacific Microwave Conference 2010*, 971–974, Yokohama, Japan, Dec. 2010.
32. Zugari, A., M. Khalladi, M. Iben Yaich, N. Raveu, and H. Baudrand, "New approach: WCIP and FDTLM hybridization," *Proc. of 2009 Mediterranean Microwave Symposium (MMS)*, 1–4, Tangiers, Morocco, Nov. 2009.
33. Girard, C., N. Raveu, S. Lanteri, and R. Perrussel, "1D WCIP and FEM hybridization," *Proc. 7th European Conference on Numerical Methods in Electromagnetism NUMELEC 2012*, 74–75, Marseille, France, Jul. 2012.
34. Harrington, R., *Applications of the Method of Moments to Electromagnetic Fields*, Cap. I, SCEEE Press, 1980.
35. Harrington, R., *Time-Harmonic Electromagnetic Fields*, Wiley-IEEE Press, 2001.
36. Jafri, A. D. U., Q. A. Naqvi, A. A. Syed, and K. Hongo, "Scattering of an arbitrarily oriented dipole field by a circular disk with surface impedance," *Progress In Electromagnetics Research*, Vol. 132, 403–424, 2012.
37. Alvarez Folgueiras, M., J. A. Rodríguez-González, and F. J. Ares-Pena, "Experimental results on a planar array of parasitic dipoles FED by one active element," *Progress In Electromagnetics Research*, Vol. 113, 369–377, 2011.